Published on
http://pselab.chem.polimi.it/

A physiologically-based diffusion-compartment model for transdermal administration – The melatonin case study

Adriana Savoca[a], Giovanni Mistraletti[b], Davide Manca[a*]

[a]*PSE-Lab*, Process Systems Engineering Laboratory, Dipartimento di Chimica, Materiali e Ingegneria Chimica "Giulio Natta", Politecnico di Milano, Piazza Leonardo da Vinci 32, 20133 Milano, ITALY
[b]Dipartimento di Fisiopatologia Medico-Chirurgica e dei Trapianti, Università degli Studi di Milano, ITALY

Published on "Computers and Chemical Engineering"
First submission: October 31st, 2017
Second submission: February 14th, 2018
Accepted: March 12th, 2018
http://dx.doi.org/10.1016/j.compchemeng.2018.03.008

ABSTRACT: There is a significant hype in the medical sector for the transdermal administration of drugs as it allows achieving a combination of multiple advantages: non-invasive procedure, pain avoidance, no first-pass hepatic metabolism, and induction of sustained plasma levels. This paper proposes a model for the study and prediction of drug transport through skin and the following distribution to human body. This is achieved by an innovative combination of the physiologically-based compartmental approach with Fick's laws of diffusion. The skin model features three strata: stratum corneum, viable epidermis, and dermis, which have a major impact on the absorption, distribution, and metabolism of transdermal drugs. The combined model accounts for skin transport via diffusion equations, and absorption and distribution in the rest of the body (i.e. organs/tissues) via material balances on homogeneous compartments. Experimental data of transdermal melatonin allow validation. Main applications are optimization of the dosage and study of skin transport.

KEYWORDS: Transdermal delivery; pharmacokinetic simulation; model sensitivity; administration route; ADME; melatonin.

Please cite this article as: ***Adriana Savoca, Giovanni Mistraletti, Davide Manca, A PHYSIOLOGICALLY-BASED DIFFUSION-COMPARTMENT MODEL FOR TRANSDERMAL ADMINISTRATION – THE MELATONIN CASE STUDY, Computers and Chemical Engineering, 113, 115–124, (2018)***
http://dx.doi.org/10.1016/j.compchemeng.2018.03.008

*Corresponding author, phone +39 02 23993271, e-mail: davide.manca@polimi.it

List of acronyms and abbreviations

ADME	Absorption, Distribution, Metabolism, and Elimination
DCPK	Diffusion-Compartment PharmacoKinetics
DE	DErmis
FDA	Food and Drug Administration
ICU	Intensive Care Unit
ODE	Ordinary Differential Equations
PB	Physiologically-Based
PBDCPK	Physiologically-Based Diffusion-Compartment PharmacoKinetics
PDE	Partial Differential Equations
SC	Stratum Corneum
TD	TransDermal
TDD	TransDermal Device
VE	Viable Epidermis

1 Introduction

Recent years have seen a rising interest in transdermal (TD) delivery as an efficient route for drug administration. Figure 1 shows the number of transdermal drugs approved by Food and Drug Administration (FDA, USA) since 1996 (FDA Orange Book, 2017).

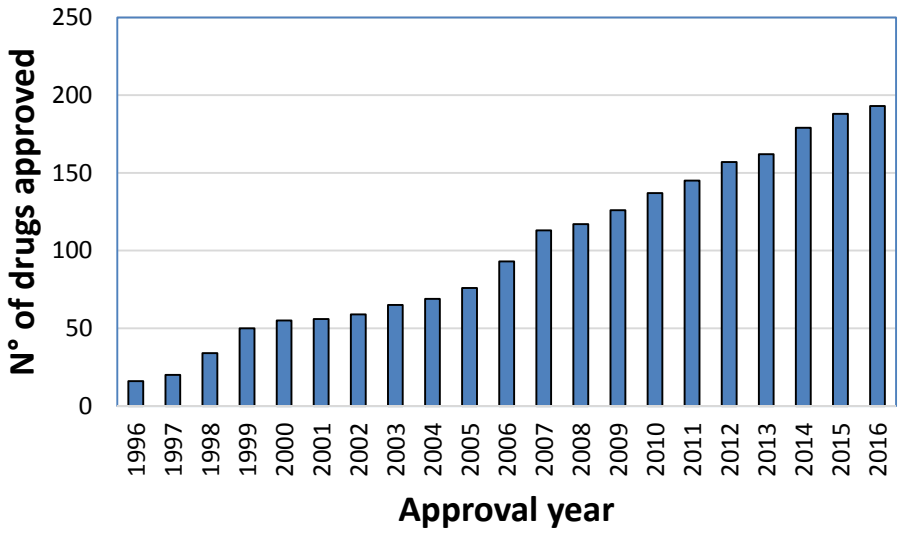

Figure 1 - Cumulative amount of transdermal drugs approved by Food and Drug Administration (FDA) since 1996 (FDA Orange Book, 2017).

This interest arises from some advantages that transdermal delivery exhibits if compared to other routes of administration (*e.g.*, enteral and parenteral). From a practical point of view, the most evident appeal of percutaneous (*i.e.* TD) delivery consists of combining a positive patient compliance with ease of administration. In fact, TD delivery does not necessarily require specialized medical staff and is non-invasive. From the pharmacokinetic point of view, the main advantage is that the drug is directly

administered to the systemic circulation. This means avoiding the first-pass hepatic metabolism, which is the main cause for the characteristic low bioavailability resulting from oral route, although some minor metabolism or binding to cellular components may occur in the skin (Prausnitz and Langer, 2008). Therefore, skin permeation is an attractive alternative whenever factors such as gastrointestinal pH, drug interaction with food, and liver diseases prevent oral administration (Mali, 2015). Furthermore, TD delivery ensures no risks of sudden fluctuations or peaks of the drug concentration in plasma, which translates into sustained levels and reduced side effects.

On the other hand, TD application comes with high inter-patient variability related to age, gender, physical characteristics, genetic factors, and living habits (Sandby-Moller et al., 2003), and is not suitable for all drugs. In fact, some physicochemical characteristics such as molecular weight and solubility may have a significant impact on the pharmacokinetics, and therefore must be taken into account when selecting the route of administration. In addition, slow absorption is another undesired pharmacokinetic trait that is intrinsic to TD administration.

In order to simulate the transdermal administration route of drugs and their distribution, metabolism, and excretion (*i.e.* ADME processes) within the human body, we developed a physiologically-based diffusion-compartment pharmacokinetic (PBDCPK) model. This dynamic model can be useful for the assessment of the optimal dosage, and in general for the development of drugs/substances for TD delivery, evaluation of toxicity/positive effects, and analysis of skin transport mechanisms.

Some authors describe skin transport by assuming stationary conditions, as their only goal is to either analyze or explain specific experimental data (Anissimov et al., 2013). Higaki et al. (2002), and Singh and Roberts (1994) developed compartment models that allow describing drugs pharmacokinetics in the skin layers, in the systemic circulation, and in some tissues of the body, *e.g.*, muscles, adipose tissue. However, they only focused on some specific tissues and did not consider the parameters governing skin transport as depending on skin depth. In fact, skin was described as a bi-layer homogenous concentration compartment. Furthermore, they did not consider the possibility of any occurring metabolism or binding.

The idea of describing skin transport as a function of both time and space is not new. In fact, Marquez-Lago et al. (2010) proposed a noteworthy 3D porous media model of the stratum corneum (*i.e.* the most superficial layer of the skin epidermis) but did not investigate the distribution in the whole human body. Kretsos et al. (2004) employed diffusion equations focused exclusively on skin penetration. This manuscript attempts to combine two aspects investigated in the literature: (i) the physiologically oriented approach towards skin transport and (ii) the attention to ADME processes within the rest of the body.

The proposed model is applied to the simulation and prediction of TD melatonin pharmacokinetics. Melatonin is a biogenic amine that is commonly found in animals, plants, and microbes. In mammals, melatonin is the main substance produced by the pineal gland (Brzezinski, 1997). In humans the endogenous production follows the day-night cycle (*aka* “circadian rhythm”), with a baseline level of about $10\ pg/mL$ during the day. Melatonin concentration starts increasing with the onset of darkness and peaks ($60-100\ pg/mL$) at 2-4 AM. Afterwards, the concentration gradually decreases and stabilizes on the daily baseline value. Several researchers are nowadays interested in melatonin numerous benefits on the human body. In humans, melatonin is regularly employed as a treatment for sleep disturbances (*e.g.*, jet lag, night-shift workers, people suffering from insomnia) (Brzezinski, 1997). Melatonin proved to benefit patients suffering from mood disorders (*e.g.*, depression, seasonal affective disorder), and neurological pathologies (*e.g.,* Alzheimer’s disease) (Hickie and Rogers, 2011; Srinivasan et al., 2006). There is some evidence of antiproliferative effects in cancer and anti-aging effects through anti-oxidant and free-radical scavenging mechanisms (Karbownik et al., 2001; Kleszczynski and Fischer, 2012; Mehta and Kaur, 2014; Srinivasan et al., 2008). A disruption of the circadian rhythm of melatonin can be observed in intensive care unit (ICU) patients (Mistraletti et al., 2010). ICU stay is thought to have a series of negative effects on patients’ sleep

and, in general, on their health status. As ICU patients’ conditions can be improved by the melatonin anti-oxidant, immunoregulatory, and sleep regulatory properties, it is possible to administer exogenous melatonin in order to restore the endogenous production rhythm. Indeed, it is desirable that the pharmacokinetics of exogenous melatonin mimics the sustained endogenous profile. Therefore, for this specific case, the previously reported advantages of the transdermal administration are convenient, and the slow absorption becomes actually a useful characteristic, despite being a drawback for most drugs. Furthermore, melatonin physicochemical characteristics (*i.e.* low molecular weight and lipophilicity) increase the probability of crossing the skin barrier.

2 Methods

2.1 Skin histology and transdermal devices

An in-depth understanding of human anatomy and physiology allows driving the engineers’ modeling activity of the transdermal administration route and correlated PBDCPK. Skin is the means for transdermal release of drugs and deserves a comprehensive insight to recognize the main mass transfer phenomena that rule their percutaneous delivery to the systemic blood flow. Human skin is the largest organ of the body and consists of three main layers: epidermis, dermis, and hypodermis (*i.e.* subcutaneous tissue). Epidermis is the thinnest and most superficial layer, and the most important for its protective function. Dermis (thickness $1.5 - 4\,mm$, Anissimov et al. (2013)) is thicker and consists of connective tissue. It contains nerves, sweat glands, hair follicles, and blood and lymphatic vessels. Hypodermis mainly consists of adipose tissue and sweat glands. Its main function is to support epidermis and dermis.

From the modeling point of view and according to the skin physiology, it is more consistent to separately consider two sublayers of the epidermis: stratum corneum (SC) (average thickness of fore-arms, face, abdomen $10 - 30\ \mu m$, Anissimov et al. (2013)) and viable epidermis (VE) (average thickness of fore-arms, face, and abdomen $50 - 100\ \mu m$, Anissimov et al. (2013)). In fact, SC is the outermost stratum and consists of a keratinized tissue, which comprises low hydrated and highly dense cell layers. For this reason, it is the most difficult to penetrate. VE is a more aqueous phase, and can be site of metabolism, binding, and active transport. In some models, it is merged with dermis, which is an aqueous medium as well (Jepps et al., 2013).

Differently from topical delivery, the goal of transdermal (or percutaneous) delivery is to pass the skin barrier and enter systemic circulation. In this case, drugs are directly applied on the skin in gel or transdermal devices (TDDs), *i.e.* patches. Hence, the amount of drug and the surface of the skin area on which the drug is applied are key parameters. Patches contain therapeutic amounts of drugs, and mainly consist of a backing for protection from the external environment and a polymeric matrix that controls the drug release. Patches often contain some penetration enhancement agents (*e.g.*, alcohols) to improve skin penetration of the drug, and other excipients (*e.g.*, adhesive). Depending on the patch, they are usually applied from one to seven days (Mali, 2015).

2.2 Skin transport equations

Our model accounts for three main layers to describe the drug concentration evolution in the skin: SC, VE, and dermis (DE). Hypodermis is neglected as the drug enters the systemic blood flow as soon as it reaches

the dermis. Diffusion is the main phenomenon involved in drug transport across skin. For this reason, we consider the drug concentration as a function of both time and skin depth x (Eq.s (1-4)).

$$\frac{\partial C_{SC}}{\partial t} = \mathfrak{D}_{SC}\ \frac{\partial^2 C_{SC}}{\partial x^2} \qquad 0 \le x < h_{SC} \tag{1}$$

$$\frac{\partial C_{VE'}}{\partial t} = \left(\mathfrak{D}_{VE}\ \frac{\partial^2 C_{VE'}}{\partial x^2}\right) - \frac{k_{EL}\, C_{VE'}}{k_M + C_{VE'}} \quad C'_{VE} = C_{VE}(1 - f_b) \qquad h_{SC} \le x < h_{VE} \tag{2}$$

$$\frac{\partial C_{DE}}{\partial t} = \mathfrak{D}_{DE}\ \frac{\partial^2 C_{DE}}{\partial x^2} \qquad h_{VE} \le x \le h_{DE} \tag{3}$$

$$\frac{\partial Q}{\partial t} = -\ \left(\mathfrak{D}_{DE}\ \frac{\partial C_{DE}}{\partial x}\right)_{x=H} \qquad H = h_{SC} + h_{VE} + h_{DE} \tag{4}$$

where $\mathfrak{D}\ [\frac{cm^2}{min}]$ is the drug diffusivity, $C\ [\frac{ng}{mL}]$ the drug concentration, and $x\ [cm]$ the axial coordinate across skin. h_{SC}, h_{VE}, h_{DE} represent the thicknesses of the three skin layers respectively, and k_{EL} and k_M are metabolism constants. $Q\ [\frac{ng}{cm^2}]$ refers to the specific amount permeated across skin. $f_b\ [-]$ quantifies the drug sequestration by viable epidermis cellular components.

The basic assumptions of the model are that (i) drug diffusion coefficients only depend on the skin depth coordinate (x), (ii) diffusion in SC is slower than diffusion in VE and DE, and (iii) diffusion velocities in VE and DE are of the same order of magnitude (Scheuplein, 1967). We accounted for metabolism in VE by introducing the Michaelis-Menten equation, that can be simplified to a first order kinetics in case $k_{EL} \gg k_M$.

The following boundary conditions complete the previous set of equations:

$$C_{DONOR} = C_{SC} \qquad t \le t_{rel} \qquad x = 0 \tag{5}$$

$$\frac{\partial C_{SC}}{\partial x} = 0 \qquad x = 0 \tag{6}$$

$$C_{SC} = k_{part1} C_{VE} \qquad \mathfrak{D}_{SC}\ \frac{\partial C_{SC}}{\partial x}\Big|_{h_{SC}^-} = \mathfrak{D}_{VE}\ \frac{\partial C_{VE}}{\partial x}\Big|_{h_{SC}^+} \qquad x = h_{SC} \tag{7}$$

$$C_{VE} = k_{part2} C_{DE} \qquad \mathfrak{D}_{VE}\ \frac{\partial C_{VE}}{\partial x}\Big|_{h_{VE}^-} = \mathfrak{D}_{DE}\ \frac{\partial C_{DE}}{\partial x}\Big|_{h_{VE}^+} \qquad x = h_{VE} \tag{8}$$

$$C_{DE} = 0 \qquad x = h_{SC} + h_{VE} + h_{DE} \tag{9}$$

Where $C_{DONOR}\ [\frac{ng}{mL}]$ is the TDD concentration (depending on the drug amount and the skin surface area covered) and $t_{rel}\ [h]$ is the duration of the drug release from the patch. k_{part1} and $k_{part2}\ [-]$ account for the phase change between layers and respectively represent the partition coefficients between SC and VE, and between VE and DE. k_{part2} is assumed 1, since there should be no discontinuity between VE and DE (Scheuplein, 1967). At $t = 0$ (*i.e.* initial conditions) the drug concentration is null in the three skin layers.

Eq. (9) is the so-called “sink condition” and accounts for the drug clearance in the innermost stratum DE, for uptake of the systemic circulation. The diffusion process is in fact supported by convective transport once the drug reaches DE, which contains blood and lymphatic vessels. Eq. (4) allows calculating the specific flux of drug permeated across skin. This flux consists of the input term R_{TD} in the plasma concentration equation:

$$R_{TD} = S_{patch}\ \frac{\partial Q}{\partial t} \tag{10}$$

$R_{TD}\ [\frac{ng}{min}]$ is the drug input rate entering the systemic circulation, and $S_{patch}\ [cm^2]$ the surface area of the TDD.

2.3 Numerical methods

The remaining organs and tissues of the human body, including the cardiovascular system (*i.e.* plasma compartment), are described with a physiologically-based pharmacokinetic (PBPK) approach: they are assimilated to perfectly stirred vessels in which the drug concentration can be considered homogenous. Thus, the mathematical model consists of material balances on these compartments (*i.e.* ordinary differential equations (ODEs)), and their numerical integration allows determining the drug pharmacokinetic evolution in the body and assessing the effect of ADME processes. The structure of the PBPK model is the same as the one proposed in Abbiati et al. (2016). However, some modifications and enhancements were added to adapt the model to different drugs and delivery routes. Indeed, Paragraph 3 provides details on the compartments added for the sake of the case-study on melatonin.

As skin pharmacokinetics depends on both time and axial coordinate, the partial derivative equations (PDEs) (Eq.s (1-4)) are discretized respect to the spatial coordinate by means of the finite differences method. The method chosen for the discretization is the central difference scheme for second-order derivatives and forward difference for first-order derivatives. The optimal number of discretization layers is 23 for each skin stratum, which results from a compromise between computational time and numerical consistency as well as precision of the solution (*i.e.* asymptotic spatial profile of the drug concentration as a function of time). This means that the final number of equations and variables (i.e. the concentration profile in the different strata) related to skin is 69. The complete model includes the ODEs of the PBPK model, whose number depends on the physical and chemical characteristics of the drug (*e.g.*, 18 for melatonin, as commented in Abbiati et al. 2016). The number of parameters does not change as a consequence of the discretization, because we assume that the diffusivity is constant for each discretization layer of the same skin stratum (Eq. (11)). Similarly, the elimination constants $k_{EL}(j)$ and $k_M(j)$ are not subject to variations throughout the discretization layers of the VE (Eq. (12) and (13)).

$$\mathfrak{D}_i(j) = \mathfrak{D}_i(j+1) \qquad i = SC, VE, DE \qquad j = 1, 2, \dots N_{layers,i} \tag{11}$$

$$k_{EL}(j) = k_{EL}(j+1) \tag{12}$$

$$k_M(j) = k_M(j+1) \tag{13}$$

As coordinate x in Eq.s (1-9) goes from 0 to the total skin thickness, H, the spatial discretization step is:

$$\Delta x_i = \frac{h_i}{N_{layers,i}} \qquad i = SC, VE, DE \tag{14}$$

The finite differences method allows converting the mathematical skin model into a system of ODEs that can be combined with the ODEs of the PBPK model.

As extensively discussed in Abbiati et al. (2016), Abbiati and Manca (2016), and Abbiati and Manca (2017), the parameters of the combined PBDCPK model are grouped into three categories: (i) individualized, (ii) assigned, and (iii) regressed. Individualized parameters can be calculated depending on some specific physical features of the patient, according to empirical correlations that can be found in the literature (*e.g.*, the volumes of organs/compartments and flowrates between them). We considered as specific features the sex, body weight, and height. Assigned parameters are some drug physicochemical properties whose value can be determined from available scientific and literature data (*e.g.*, protein binding). Some parameters can be neither found in the literature nor calculated by empirical correlations (*e.g.*, diffusivity, transfer coefficients, metabolic constants), thus they are computed via a non-linear regression procedure respect to experimental data. In particular, the objective function of the non-linear regression procedure is the squared difference between the experimental (Benes et al., 1997 for the proposed case-study) and predicted values of the concentrations. For the sake of correctness, we acknowledge that the value of some transfer coefficients might be determined from *in vitro* studies. However, *in vitro* experiments do not take

into account the interactions among organs and tissues in the full living organism, which dramatically affect the resulting values.

2.4 Sensitivity analysis

We performed a local sensitivity analysis to assess the influence of the model adaptive parameters on the concentration of the most representative compartments. We calculated the normalized sensitivity matrix $\boldsymbol{S}$, whose elements consist of the normalized derivatives of the concentrations $C(t)$ respect to the regressed parameters p of the model:

$$\boldsymbol{S} = \frac{\boldsymbol{p}}{\boldsymbol{C}(t)} \frac{\partial \boldsymbol{C}(t)}{\partial \boldsymbol{p}} \tag{15}$$

Since the model is dynamic we carried out the sensitivity analysis at the most critical time points from the pharmacokinetic point of view, *i.e.* (i) immediately after drug administration, (ii) at $t = t_{MAX}$ (time corresponding to the experimental maximum concentration, C_{MAX}), and (iii) immediately after the end of the patch release time. Section 4 (see also Figure 2) discusses the most significant results at $t = t_{MAX}$.
The derivatives in Eq. (15) are approximated by means of the finite differences method. The perturbation on the parameters is:

$$\Delta \boldsymbol{p} = |\boldsymbol{p}| \cdot \varepsilon_r + \varepsilon_a \tag{16}$$

Where ε_r, the relative tolerance, is optimally set to the square root of the macheps constant, and ε_a, the absolute tolerance, is suitably chosen as the macheps constant.

3 Case study: melatonin

Several melatonin applications (*e.g.*, ICU patients, jetlag, insomnia) call for reaching sustained and physiological plasma levels of such a substance. These goals can be achieved by transdermal delivery. In fact, orally administered melatonin is characterized by short half-life of elimination ($40 - 60\ min$, (DeMuro et al., 2000; Gooneratne et al., 2012)) and low bioavailability because of the first-pass hepatic metabolism. Furthermore, because of its lipophilic characteristics, melatonin can cross the SC hydrophobic barrier. Its low molecular weight ($232.278\ {}^{g}/_{mol}$) contributes to ensuring fast diffusion.
The skin transport equations reported above can therefore be adapted to melatonin. We accounted for melatonin metabolism in VE with a first-order elimination constant. In fact, although skin metabolism certainly occurs via an enzymatic mechanism, we chose not to use the Michaelis-Menten equation. Indeed, the Michaelis-Menten parameters are related to specific enzymes involved in the metabolic process, but the tissue contribution to melatonin metabolism is still not fully assessed and clarified. Therefore, we decided upon avoiding the introduction of an additional adaptive parameter that should be identified via the non-linear regression procedure. Furthermore, the assumption of first-order kinetics is not unrealistic, as in many applications $k_{EL} \gg k_M$. Likewise, the scientific literature (Slominski et al., 2012) reports the presence of melatonin receptors in skin, which are involved in some skin-related physiological (*e.g.*, regulation of skin pigmentation, hair growth) and pathophysiological processes (*e.g.*, melanoma growth). However, there are no literature findings that quantify the melatonin binding in the skin. For this reason, we neglected the binding fraction f_b. If further details become available in the literature, the model will be re-adapted accordingly. As we explain in Section 2.3, ADME processes in the body are described via ODEs according to Abbiati et al. (2016). In particular, the PBPK model features 8 compartments: Plasma, Gastric

Lumen (GL), Small Intestinal Lumen (SIL), Large Intestinal Lumen (LIL), Liver, Gastro-Intestinal Circulatory System (GICS), Poorly perfused Tissues (PT), and Highly perfused Organs (HO).

We added two more compartments to adapt to melatonin pharmacokinetic properties, *i.e.* the salivary glands and the pineal gland (Eq. (17), and Eq. (18), respectively). It is known that a non-negligible amount of melatonin diffuses from plasma to saliva. Indeed, several experimental studies assess the melatonin amount in the human body by measuring both plasma and saliva concentrations or, in some cases, only saliva (Benloucif et al., 2008; Laakso et al., 1993; Voultsios et al., 1997). The pineal gland is added because it is the source of endogenous melatonin in mammals (Brzezinski, 1997). Eq. (19) describes the dynamic evolution of melatonin's main metabolite 6-sulfatoxymelatonin ($aMT6s$) concentration in plasma.

$$\frac{dC_{PG}}{dt} = \frac{1}{V_{PG}} \left(Qin_{PG} C_P - Qout_{PG} C_{PG} + r_{prod}(T)\right) \quad (17)$$

$$\frac{dC_{SA}}{dt} = \frac{1}{V_{SA}} Q_{sal} C_P - k_{sal} C_{SA} \quad (18)$$

$$\frac{dC_{aMT6s}}{dt} = \frac{1}{V_P} (0.9\, CL_H C_L - CL_K C_{aMT6s}) \quad (19)$$

Where V_{PG}, V_{SA}, and $V_P\,[mL]$ are the volumes of the pineal gland, salivary glands, and plasma compartments, respectively, Qin_{PG}, $Qout_{PG}$, $Q_{sal}\,[\frac{ng}{mL}]$ are the blood flowrates entering/exiting the corresponding compartments, $k_{sal}\,[min^{-1}]$ is the saliva-plasma transfer coefficient. CL_H and $CL_K\,[\frac{mL}{min}]$ are the hepatic and renal clearances, where 90% is the average percentage of melatonin that the liver converts into $aMT6s$ (Karasek and Winczyk, 2006), which is eventually eliminated by kidneys. For the sake of simplicity, and for the lack of quantitative information in the literature, we consider only the hepatic metabolism, although we are aware that some $aMT6s$ is produced in skin and other tissues (Pandi-Perumal et al., 2006). $r_{prod}(T)$ is the production rate of endogenous melatonin in the pineal gland, which is entrained with the day-night cycle ($T = 24\,h$). This term consists of a Fourier series truncated to the second term to account for the periodicity of secretion. The Fourier coefficients are determined via a separate nonlinear regression respect to suitable experimental data of the endogenous melatonin concentration (Voultsios et al., (1997)). It is possible to employ this strategy for any endogenous substance that follows the circadian rhythm, *e.g.*, corticosteroids.

We employed experimental data of plasma melatonin and $aMT6s$ concentration from Benes et al. (1997) to identify the parameters of the diffusion-compartment model. They used a $20\,cm^2$ patch loaded with $8\,mg$ of melatonin and administered to 12 healthy volunteers. Averaged demographic and experimental data of the group of patients are available in that article.

4 Results and discussion

Preliminary to the regression with experimental data, we investigated the influence of some key parameters on the amount of permeated drug across skin and the plasma concentration profile. In particular, we focused our attention on the variation of the SC diffusivity $\mathfrak{D}_{SC}$ and the SC/VE partition coefficient k_{part1}. Figure 2 shows the results of this analysis in terms of specific drug amount (A), melatonin and aMT6s plasma concentration (B, C), and SC layers concentration (D,E, and F) trends.

In Figure 2 (top panel) SC diffusivity $\mathfrak{D}_{SC}$ varies from 10^{-6} to $10^{-3}\,[\frac{cm^2}{min}]$ while the partition coefficient k_{part1} is kept constant at $2\,[-]$. As expected, if the diffusivity value is too low, no drug can permeate and reach the systemic circulation. In particular, the lowest value of the SC diffusivity $\mathfrak{D}_{SC}$ (blue curve) results

in such a slow absorption in skin that the resulting plasma concentration (Figure 2 B and C, top panels) and permeated drug amount (Figure 2 A, top panels) are practically null. For higher values, the skin absorption (Figure 2 D, E, and F, top panels) increases significantly and this leads to higher plasma concentration and permeated drug amount.

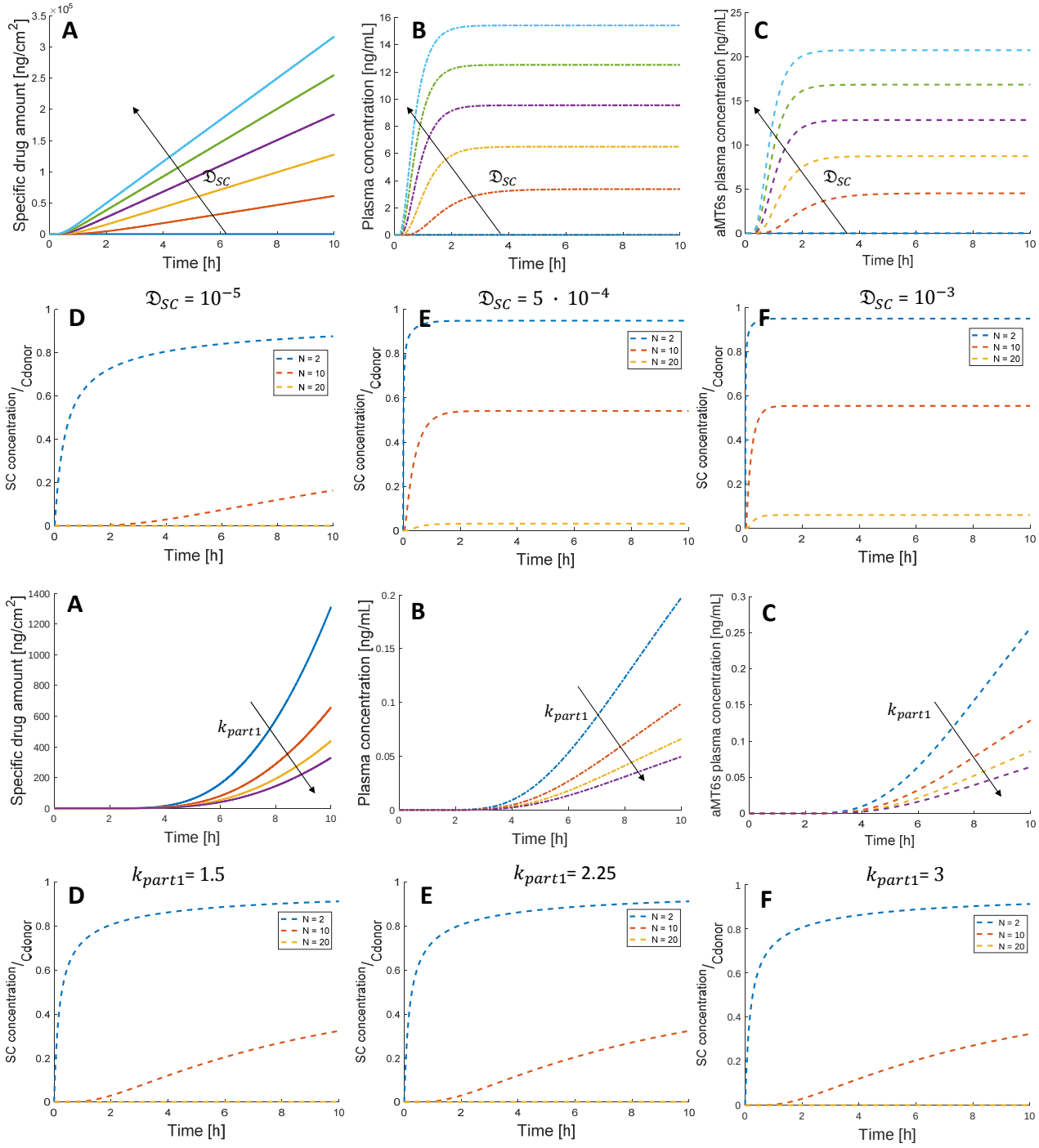

Figure 2 –Trends of (A) amount of drug permeated, and (B, C) resulting plasma concentration for increasing values of $\mathfrak{D}_{SC}$ (top panels) and k_{part1} (bottom panels).Graphs D, E, F show the trends of the concentration in specific SC layers for different values of $\mathfrak{D}_{SC}$ (top panels) and k_{part1} (bottom panels). $\mathfrak{D}_{SC}$ varies in the 10^{-6} to 10^{-3}[cm^2/min] interval, while k_{part1}varies in the 1.5 to 3 [−] interval.

Afterwards, we studied the influence of the SC/VE partition coefficient k_{part1} (values from 1.5 to 3 [−]) at $\mathfrak{D}_{SC} = 10^{-5}$ [$\frac{cm^2}{min}$] (see Figure 2, bottom panels). The increase of the SC/VE partition coefficient lowers

VE (and DE) concentrations and, consequently lowers the plasma levels (Figure 2 B and C, bottom panels), while having smaller influence on the SC concentration. As far as the parameters identification is concerned, the nonlinear regression procedure achieves acceptable results (see Figure 3), as the simulated melatonin plasma curve is near to the central values of the experimental measures (left panel). On the other hand, the model simulation underestimates the experimental metabolite $aMT6s$ plasma concentration (right panel) before the experimental concentration peak. This result can be attributed to some simplifying assumptions that we made about the melatonin metabolism. In fact, we considered $aMT6s$ as the only metabolite, and we did not consider the intermediate reactions and products in the metabolic scheme of melatonin. The metabolite equation, Eq. (19), accounts for the metabolism in the liver, although we are aware that metabolism occurs also in skin and other tissues. As it is not clear which tissues play a role in melatonin metabolism, and to what extent, we chose to make a compromise between real physiology and model complexity, and consider only the liver.

The experimental trend of Figure 3 shows that the velocity of the distribution-elimination phase (after the experimental concentration peak C_{MAX} the 13th hour) is slower compared to the velocity of the uptake in the systemic circulation (preceding the experimental concentration peak C_{MAX} at the 13th hour). This occurs also because of the onset of melatonin endogenous secretion from the pineal gland (note the “Real time of day”, on the top x axis and the black vertical dashed line), which our model can take into account. The wide error bars in the experimental data confirm high inter-individual variability.

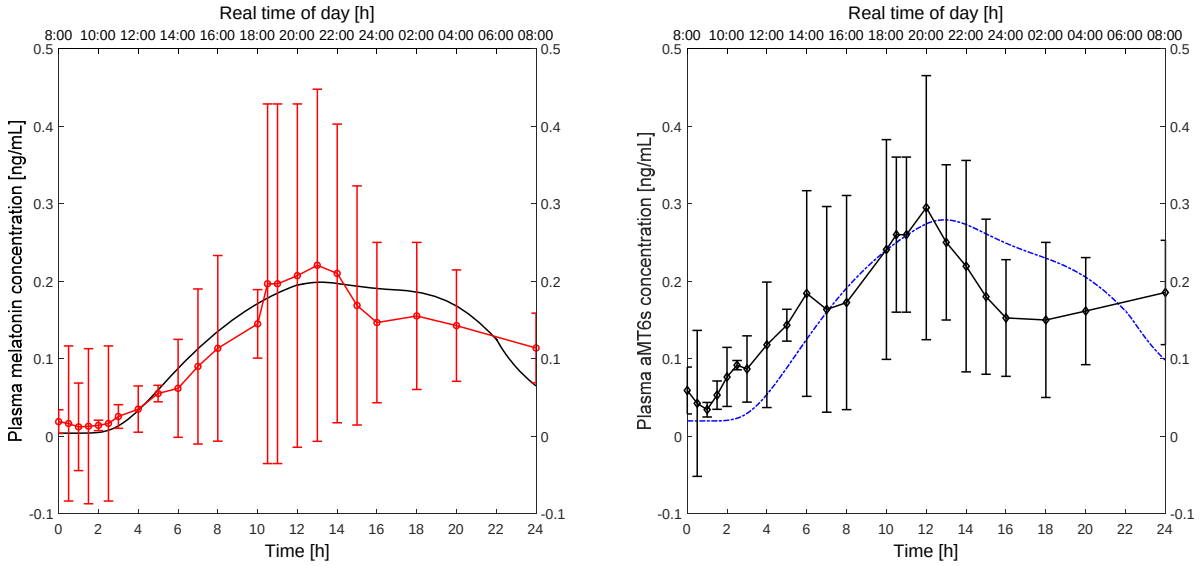

Figure 3 – Results of the regression procedure for identification of PBDCPK model parameters. Experimental data (Benes et al., 1997) show the evolution of melatonin concentration (left panel, red circles) and $aMT6s$ concentration (right panel, black diamonds) in plasma. The continuous smooth curves represent the corresponding simulated results. The model curve is quite near to the central values of the error bands for most of the experimental sampled values of melatonin plasma concentration. The experimental $aMT6s$ concentration is underestimated, consistently with the simplifying mechanistic assumptions on the metabolism. The black vertical dashed line shows the time of onset of endogenous melatonin production.

Figure 4 shows the single and total contributions of plasma melatonin as predicted by the proposed model: blue dash-dotted line shows the exogenous melatonin contribution while dashed red line shows the endogenous contribution. The black continuous curve comes from the combination of the two. Three black dotted vertical lines show (i) the end of application time of the TDD, (ii) the onset of melatonin endogenous secretion by pineal gland, and (iii) the endogenous predicted peak (at 4 AM). It is interesting to notice that after the end of the time of application of the patch the exogenous curve keeps increasing for a while (*i.e.* about 3 h) as skin behaves as a reservoir. The fact that we are considering the pineal gland as the only

organ capable of secreting melatonin can contribute explaining the underestimation of the experimental data observable after the 20th hour (Figure 3, left panel). In fact, although it is acknowledged in the literature that other tissues have a smaller contribution to melatonin secretion (Huether,1993; Conti et al., 2000; Kleszczynski and Fischer,2012), their extent is not yet quantified.

It is worth observing that the values of the regressed parameters are consistent with the preliminary hypotheses and with both the skin anatomy and physiology, as the SC diffusivity is indeed lower than VE and DE diffusivities, which instead assume the same order of magnitude (see also Table 1).

Table 1 – Values of the skin equation parameters identified by the regression procedure. They denote consistency with the basic model hypotheses and the anatomy/physiology of the human patients. Last two columns list the 90% bootstrap confidence intervals (CI) of the skin equation parameters.

Parameters	Description	Regressed values	90% CI_{lb}	90% CI_{ub}
$\mathfrak{D}_{SC}\ [cm^2/min]$	SC Diffusivity	$3.352 * 10^{-5}$	$1.269 * 10^{-5}$	$5.431 * 10^{-5}$
$\mathfrak{D}_{VE}\ [cm^2/min]$	VE Diffusivity	$5.943 * 10^{-3}$	$2.122 * 10^{-3}$	$9.763 * 10^{-3}$
$\mathfrak{D}_{DE}\ [cm^2/min]$	DE Diffusivity	$2.776 * 10^{-3}$	$1.395 * 10^{-3}$	$6.946 * 10^{-3}$
$k_{part1}\ [-]$	SC/VE Partition coefficient	1.763	1.209	2.317

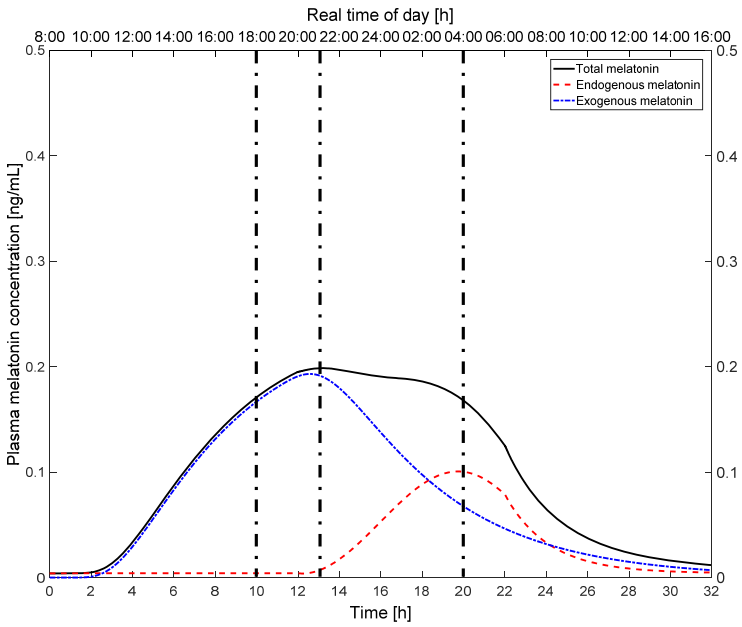

Figure 4 – Trends of the single and total contributions of plasma melatonin pharmacokinetics. Dashed red line curve shows the endogenous melatonin pharmacokinetic profile, with onset indicated by a dash-dotted black line. Dash-dotted blue line shows the pharmacokinetic profile of TD exogenous melatonin. Black vertical lines indicate respectively (i) the end of application of the TDD, (ii) the onset of endogenous production, and (iii) the peak of endogenous melatonin.

Figure 5 shows the simulation of the pharmacokinetic profile resulting from administration of melatonin $5\ mg$ by a $10\ cm^2$ patch, which is removed after $8\ h$. The simulated patient does not exhibit endogenous melatonin production. The resulting model plasma concentration (Figure 5, right panel, blue continuous curve) is comparable to the endogenous profile of melatonin in healthy human beings (experimental data in black circles from Voultsios et al., 1997). The model can in fact be employed to study and simulate the resulting pharmacokinetic profile of transdermal melatonin for administration to patients who manifest

endogenous production disruption, *i.e.* ICU patients, people suffering from insomnia or jet-lag, and night-shift workers. This result can be achieved by dose optimization.

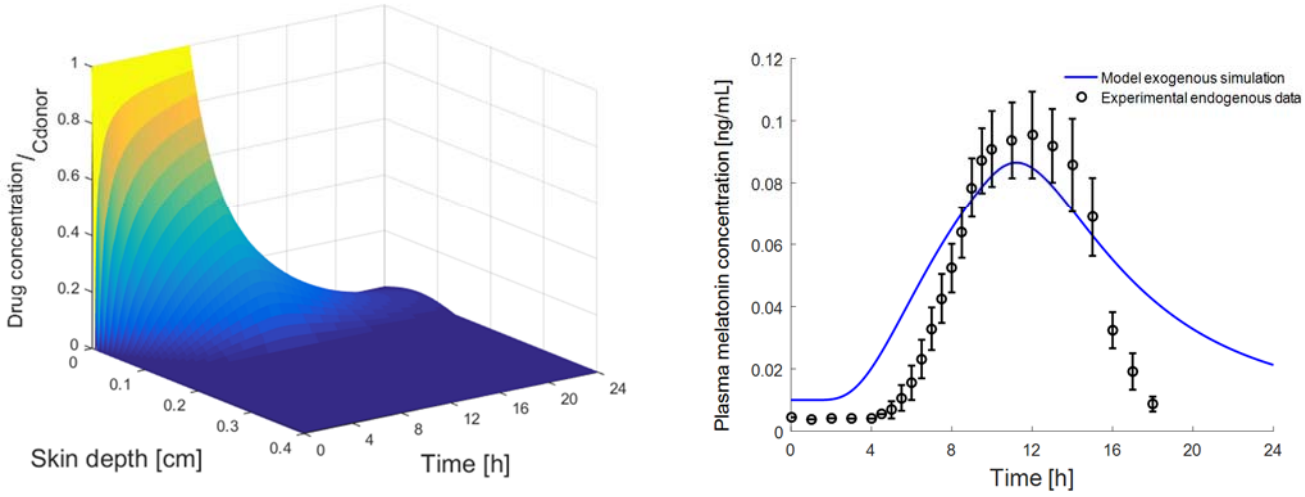

Figure 5 – (Left panel) Skin concentration profiles. x-axis represents skin depth $[cm]$, while y-axis represents time $[h]$. z-axis shows the ratio between the drug concentration in skin strata and the donor concentration, *i.e.* TDD concentration. As expected, SC exhibits drug accumulation, while DE concentration is very low. We can observe the effect of SC that plays the role of reservoir towards the end of the simulation. (Right panel) Simulated profile of plasma concentration (blue continuous curve) after TD administration in a patient with no endogenous production, compared with experimental data (black circles) of endogenous levels in healthy human beings (Voultsios et al., (1997)). It is evident that TD administration is a valid option to reproduce melatonin endogenous profile.

On the left panel, we show the evolution of melatonin concentration along the skin depth (x-axis) and in time (y-axis). The pharmacokinetic profile exhibits melatonin accumulation within SC, and very low levels in DE. The reservoir function of SC produces a small increase towards the end of administration, even after the end of release from the transdermal device. Unfortunately, it is not possible to validate the results of the permeated drug amount and the concentration in the skin layers (see Figure 5, left panel), as it is not feasible to obtain this piece of information during *in vivo* experiments in humans. However, the order of magnitude of the permeated drug amount is consistent with the experimental results of Dubey et al. (2007) on melatonin permeation across human cadaver skin (*ex vivo*). Consistent with expectations, we observed that SC is the main resistance to skin transport, while the concentration levels in DE are very low compared to those of the other two strata, because of the continuous clearance of the blood supply. Lower concentration in VE respect to adjacent SC is explained by the presence of metabolism.

Figure 6 shows a distinct experimental case-study for validation purposes. Aeschbach et al. (2009) administered melatonin $2.1\,mg/1.2\,cm^2$ as patch. The purpose of the study was to show that TD administration of melatonin can reduce awakening after sleep onset and therefore improve sleep maintenance. The reported demographic data consist only of averaged measures of the subjects’ group, thus the black continuous curve is the pharmacokinetics of an averaged individual simulated by the model, while the circles are the experimental values of melatonin concentration of the individuals who took part to the study. It is worth observing that the model curve is consistently near to three out of four individual trends. The most distant individual trend (orange circles) shows abnormal pharmacological levels, probably related to differences in the skin characteristics. The sensitivity analysis provided some insights on the influence of the most representative parameters on the model variables. Figure 7 (top panel) shows the

sensitivity of skin diffusivities $\mathfrak{D}_{SC}, \mathfrak{D}_{VE}$, and $\mathfrak{D}_{DE}$ on (i) melatonin (M) concentration (at $t = t_{MAX}$) in intermediate layers of SC, VE, DE, and in plasma and liver, and (ii) $aMT6s$ concentration (at $t = t_{MAX}$) in plasma.

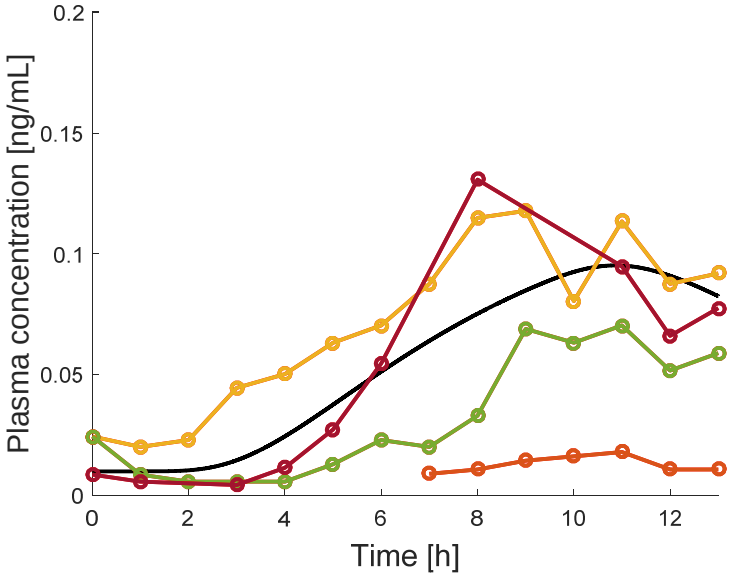

Figure 6 –The colored circles and trends represent the plasma pharmacokinetics of transdermal melatonin in four healthy individuals (Aeschbach et al., 2009). The black continuous curve depicts the simulated melatonin pharmacokinetics of an averaged in-silico individual.

$\mathfrak{D}_{VE}$ seems to be the most sensitive parameter for the concentration in skin layers, while the effect of $\mathfrak{D}_{DE}$ is less evident. This particular point allows remarking that the sensitivity indexes calculation depends considerably on the punctual ($t = t_{MAX}$) value of the concentration (see Eq. (15)).

Figure 7 (medium panel) shows the results of the sensitivity analysis of the same variables at same time ($t = t_{MAX}$) respect to the parameters that characterize the liver, hepatic, and skin metabolism. Consistently with the model structure and hypotheses, Eff_K is the most sensitive parameter for plasma aMT6s concentration, as it is the parameter governing renal clearance of the metabolized drug. Similarly, Eff_H variation significantly affects liver concentration, while the skin metabolic constant k_{EL} sensitivity index is smaller compared to the renal and kidneys efficiencies. In fact, the tissue contribution to melatonin metabolism/elimination process is less significant than the contribution exerted by the liver and kidneys. It is worth remarking that although VE is the stratum where skin metabolism occurs, the concentration in VE is not the most affected one by k_{EL} variation.

Figure 7 (bottom panel) shows sensitivity indexes values of the partition coefficients k_{part1} and k_{part2}. Both are sensitive respect to all the key model variables, especially plasma and liver concentration. This result may be seen as a warning, considering that we have assigned k_{part2} equal to 1. Despite this result, we think that it is more sensible to try and reduce the degrees of freedom of the nonlinear regression by assigning some of the unknown parameter values based on hypotheses resting on physiology. Therefore, we stand by our decision of assigning k_{part2}.

The method employed for the sensitivity analysis allows observing the influence of variation of only one parameter at a time. A more in-depth future investigation would require a global sensitivity analysis implying that all the parameters vary at the same time, which may be a more likely situation in a biological system such as the human body subject to some clinical treatment.

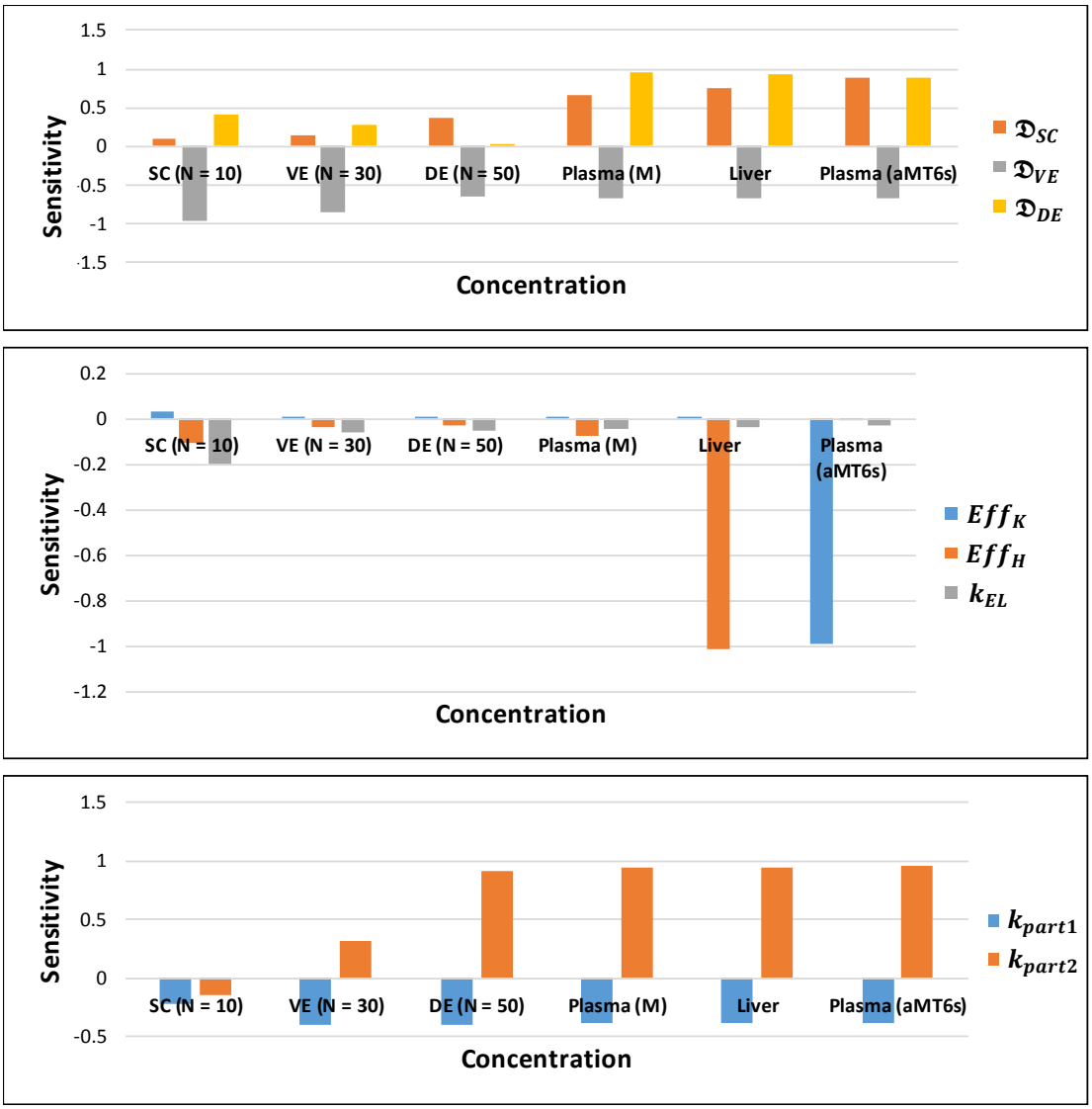

Figure 7 – Local sensitivity analysis of skin strata diffusivities (top panel), elimination/metabolic constants (medium panel), and partition coefficients (bottom panel). Model variables considered are the melatonin (M) concentration in SC, VE, DE, plasma, and liver, and the metabolite ($aMT6s$) concentration in plasma. The analysis is carried out at $t = t_{MAX}$.

5 Conclusions

The proposed PBDCPK model can be employed for the simulation and prediction of the pharmacokinetics resulting from percutaneous administration of drugs and specifically of melatonin. The model identification procedure based on non-linear parametric regression provided results consistent with the physiology of human body. In spite of high inter-individual variability, the validation shows that the model can be used to predict averaged patient transdermal melatonin pharmacokinetics. *In silico* simulations are an effective and costless tool for studies on skin transport, dose optimization, and route of administration selection. In fact, compared to other models describing percutaneous absorption, this work overcomes some simplifying assumptions *e.g.*, one- or two-layer approximation, not physiologically-based pharmacokinetic model (Cevc and Vierl, 2007), stationary (*i.e.* steady-state) assumptions (Anissimov et al., (2013)), and homogeneous

concentration in skin (Higaki et al., 2002). As a final remark, it would be interesting to include a release kinetics in our model dependent on the type of transdermal device employed.

As a consequence of the increased interest in melatonin in several medical fields, such as treatment of ICU patients, it would be interesting to focus on some recurring features of those subjects (*e.g.*, hypoperfusion, hepatic diseases, renal failure, gastro-intestinal disturbs, inflammation). Indeed, the capability of the model to describe ICU patients for TD administration and the resulting PK would strengthen the versatility attribute of the proposed model and its predictive reliability.

The main challenge is represented by inter- and intra-patient variability of the pharmacokinetics. Future work will see the model as a tool for the selection of the optimal dose/formulation. Inter-individual variability may in fact be tackled with a scenario-based approach for optimization. Artificially generated scenarios of virtual patients would help account for the stochastic uncertainty that comes from different physical characteristics, genetics, gender, race, and the resulting impact on pharmacokinetics.

References

Abbiati, R.A., Lamberti, G., Grassi, M., Trotta, F., Manca, D. (2016). Definition and validation of a patient-individualized physiologically-based pharmacokinetic model. Computers & Chemical Engineering, 84, 394-408.

Abbiati, R.A., Manca, D. (2016). A modeling tool for the personalization of pharmacokinetic predictions. Computers & Chemical Engineering, 91, 28-37.

Abbiati, R.A., Manca, D. (2017). Innovations and Improvements in Pharmacokinetic Models Based on Physiology. Curr Drug Deliv, 14, 190-202.

Aeschbach, D., Lockyer, B.J., Dijk, D.J., Lockley, S.W., Nuwayser, E.S., Nichols, L.D., Czeisler, C.A. (2009). Use of transdermal melatonin delivery to improve sleep maintenance during daytime. Clin Pharmacol Ther, 86, 378-382.

Anissimov, Y.G., Jepps, O.G., Dancik, Y., Roberts, M.S. (2013). Mathematical and pharmacokinetic modelling of epidermal and dermal transport processes. Adv Drug Deliv Rev, 65, 169-190.

Benes, L., Claustrat, B., Horriere, F., Geoffriau, M., Konsil, J., Parrott, K.A., DeGrande, G., McQuinn, R.L., Ayres, J.W. (1997). Transmucosal, oral controlled-release, and transdermal drug administration in human subjects: a crossover study with melatonin. J Pharm Sci, 86, 1115-1119.

Benloucif, S., Burgess, H.J., Klerman, E.B., Lewy, A.J., Middleton, B., Murphy, P.J., Parry, B.L., Revell, V.L. (2008). Measuring Melatonin in Humans. Journal of Clinical Sleep Medicine : JCSM : official publication of the American Academy of Sleep Medicine, 4, 66-69.

Brzezinski, A. (1997). Melatonin in humans. N Engl J Med, 336, 186-195.

Cevc, G., Vierl, U. (2007). Spatial distribution of cutaneous microvasculature and local drug clearance after drug application on the skin. J Control Release, 118, 18-26.

Conti, A., Conconi, S., Hertens, E., Skwarlo-Sonta, K., Markowska, M., & Maestroni, G. J. M. (2000). Evidence for melatonin synthesis in mouse and human bone marrow cells. Journal of Pineal Research, 28, 193-202.

DeMuro, R.L., Nafziger, A.N., Blask, D.E., Menhinick, A.M., Bertino, J.S., Jr. (2000). The absolute bioavailability of oral melatonin. J Clin Pharmacol, 40, 781-784.

Dubey, V., Mishra, D., Jain, N.K. (2007). Melatonin loaded ethanolic liposomes: Physicochemical characterization and enhanced transdermal delivery. European Journal of Pharmaceutics and Biopharmaceutics, 67, 398-405.

Food and Drug Administration (FDA) Orange Book (2017). Approved Drug Products with Therapeutic Equivalence Evaluations. Silver Spring, MD 20993.

Gooneratne, N.S., Edwards, A.Y., Zhou, C., Cuellar, N., Grandner, M.A., Barrett, J.S. (2012). Melatonin pharmacokinetics following two different oral surge-sustained release doses in older adults. J Pineal Res, 52, 437-445.

Hickie, I.B., Rogers, N.L. (2011). Novel melatonin-based therapies: potential advances in the treatment of major depression. The Lancet, 378, 621-631.

Higaki, K., Asai, M., Suyama, T., Nakayama, K., Ogawara, K., Kimura, T. (2002). Estimation of intradermal disposition kinetics of drugs: II. Factors determining penetration of drugs from viable skin to muscular layer. Int J Pharm, 239, 129-141.

Huether, G. (1993). The contribution of extrapineal sites of melatonin synthesis to circulating melatonin levels in higher vertebrates. Experientia, 49, 665-670.

Jepps, O.G., Dancik, Y., Anissimov, Y.G., Roberts, M.S. (2013). Modeling the human skin barrier – Towards a better understanding of dermal absorption. Adv Drug Deliv Rev, 65, 152-168.

Karasek, M., Winczyk, K. (2006). Melatonin in humans. J Physiol Pharmacol, 57 Suppl 5, 19-39.

Karbownik, M., Lewinski, A., Reiter, R.J. (2001). Anticarcinogenic actions of melatonin which involve antioxidative processes: comparison with other antioxidants. Int J Biochem Cell Biol, 33, 735-753.

Kleszczynski, K., Fischer, T.W. (2012). Melatonin and human skin aging. Dermato-endocrinology, 4, 245-252.

Kretsos, K., Kasting, G.B., Nitsche, J.M. (2004). Distributed diffusion–clearance model for transient drug distribution within the skin. J Pharm Sci, 93, 2820-2835.

Laakso, M.-L., Hätönen, T., Stenberg, D., Alila, A., Smith, S. (1993). One-hour exposure to moderate illuminance (500 lux) shifts the human melatonin rhythm. Journal of Pineal Research, 15, 21-26.

Mali, A.D. (2015). An updated review on transdermal drug delivery systems. skin, 8, 9.

Marquez-Lago, T.T., Allen, D.M., Thewalt, J. (2010). A novel approach to modelling water transport and drug diffusion through the stratum corneum. Theoretical Biology and Medical Modelling, 7, 33.

Mehta, A., Kaur, G. (2014). Potential role of melatonin in prevention and treatment of oral carcinoma. Indian Journal of Dentistry, 5, 86-91.

Mistraletti, G., Sabbatini, G., Taverna, M., Figini, M.A., Umbrello, M., Magni, P., Ruscica, M., Dozio, E., Esposti, R., DeMartini, G., Fraschini, F., Rezzani, R., Reiter, R.J., Iapichino, G. (2010). Pharmacokinetics of orally administered melatonin in critically ill patients. J Pineal Res, 48, 142-147.

Pandi-Perumal, S. R., Srinivasan, V., Maestroni, G. J., Cardinali, D. P., Poeggeler, B., & Hardeland, R. (2006). Melatonin: Nature's most versatile biological signal? FEBS J, 273, 2813-2838.

Prausnitz, M.R., Langer, R. (2008). Transdermal drug delivery. Nature biotechnology, 26, 1261-1268.

Sandby-Moller, J., Poulsen, T., Wulf, H.C. (2003). Epidermal thickness at different body sites: relationship to age, gender, pigmentation, blood content, skin type and smoking habits. Acta Derm Venereol, 83, 410-413.

Scheuplein, R.J. (1967). Mechanism of Percutaneous Absorption: II. Transient Diffusion and the Relative Importance of Various Routes of Skin Penetration**From the Research Laboratories of the Department of Dermatology of the Harvard Medical School at the Massachusetts General Hospital, Boston, Massachusetts 02114. Journal of Investigative Dermatology, 48, 79-88.

Singh, P., Roberts, M.S. (1994). Skin permeability and local tissue concentrations of nonsteroidal anti-inflammatory drugs after topical application. J Pharmacol Exp Ther, 268, 144-151.

Slominski, R.M., Reiter, R.J., Schlabritz-Loutsevitch, N., Ostrom, R.S., Slominski, A.T. (2012). Melatonin membrane receptors in peripheral tissues: Distribution and functions. Mol Cell Endocrinol, 351, 152-166.

Srinivasan, V., Pandi-Perumal, S.R., Cardinali, D.P., Poeggeler, B., Hardeland, R. (2006). Melatonin in Alzheimer's disease and other neurodegenerative disorders. Behavioral and Brain Functions, 2, 15-15.

Srinivasan, V., Spence, D.W., Pandi-Perumal, S.R., Trakht, I., Cardinali, D.P. (2008). Therapeutic actions of melatonin in cancer: possible mechanisms. Integr Cancer Ther, 7, 189-203.

Voultsios, A., Kennaway, D.J., Dawson, D. (1997). Salivary melatonin as a circadian phase marker: validation and comparison to plasma melatonin. J Biol Rhythms, 12, 457-466.